Bioorganic Chemistry 91 (2019) 103154

Contents lists available at ScienceDirect

Bioorganic Chemistry

journal homepage: www.elsevier.com/locate/bioorg

Tyrosine-based asymmetric urea ligand for prostate carcinoma: Tuning biological efficacy through *in silico* studies

Sagnik Sengupta[a], Mena Asha Krishnan[b], Amit Pandit[a], Premansh Dudhe[a], Rajesh Sharma[c], Venkatesh Chelvam[a,b,*]

[a] Discipline of Chemistry, Indian Institute of Technology Indore, Khandwa Road, Simrol, Indore 453 552, India
[b] Discipline of Biosciences and Biomedical Engineering, Indian Institute of Technology Indore, Khandwa Road, Simrol, Indore 453 552, India
[c] School of Pharmacy, Devi Ahilya University, Takshshila Campus, Khandwa Road, Indore 452 017, India

ARTICLE INFO

Dedicated to Prof. Hiriyakkanvar Ila, JNCASR, Bangalore on the occasion of her 75th Birth Anniversary.

Keywords:
In silico
Tyrosine-based urea ligands
PSMA
In vitro study
Diagnostic probe

ABSTRACT

In this article, we have explored the chemical interactions of tyrosine-based asymmetric urea ligands in the binding pockets of prostate specific membrane antigen (PSMA) through *in silico* studies. The S1 pocket of the PSMA protein offers better scope for modifications in the urea ligands to improve the binding affinity. Accordingly, tyrosine-based (S)-2-(3-((S)-1-carboxy-2-(4-(carboxymethoxy)phenyl)ethyl)ureido)pentanedioic acid (CYUE, **3**) ligand was designed, synthesized and predicted to possess inhibition constant (Ki) of 55 nM with PSMA protein. The CYUE (**3**) ligand was further elaborated into a fluorescent diagnostic probe for detection of $PSMA^+$ cancers. *In vitro* studies on human malignant cell lines such as LNCaP and PC-3 were performed to show the efficacy and specificity of the newly synthesized bio-construct. The fluorescent bio-conjugate was found to be very specific to the PSMA protein with an overall binding affinity constant (K_D) of 88 nM.

1. Introduction

Prostate cancer (PCa) is the second most diagnosed malignancy after lung cancer in western countries [1]. Cancer statistics on PCa depicts 164,690 newly diagnosed cases and 29,430 estimated deaths in the calendar year of 2018 [2]. The available diagnostic techniques for the detection of PCa are digital rectal examination, blood prostate-specific antigen (PSA) measurement, and ultrasound-guided prostate biopsy [3]. Despite the successful adaption of these diagnostic modalities for detecting PCa, the methods have several disadvantages [4–6], leaving most early malignancies and sites of metastasis in advanced disease undetected, for which complementary or alternative diagnostic methods are needed. Targeting biomarkers over-expressed during pathological diseased state such as cancer is one of the reliable ways to diagnose as well as to treat the disease [7]. Therefore, identification of specific biomarkers is strongly recommended so that the patients receive appropriate treatment at an early stage before the advancement of the disease.

Prostate specific membrane antigen (PSMA also known as Glutamate carboxypeptidase II or GCP II) is an integral membrane protein (binuclear zinc peptidase) present in the prostate epithelial cells and upregulated to several folds in high-grade, metastatic and androgen-insensitive prostate carcinomas [8,9]. It is pertinent to understand the architecture of PSMA binding site, and its interaction with the natural ligand i.e. *N*-acetyl-aspartyl-glutamate (NAAG), for the design and development of a new small molecule inhibitors of PSMA. The active site of PSMA consists [10] of two binding pockets (S1 and S1′) and the interactions of NAAG with this cavity shows that the glutamate functionality of NAAG interacts with the S1′ pocket while the rest of the inhibitor interacts with the S1 pocket. Glutamic acid-based urea inhibitors [11,12], glutamic lysine-based urea heterodimers [13–18] and phosphoramidates [19–22] are well documented small molecule inhibitors which are proved to be highly specific towards PSMA. These molecules have shown excellent activity *in vitro* and *in vivo* studies and generally considered as potential clinical candidates for the treatment and diagnosis of early malignancy of prostate gland.

In this study, we have opted for the development of an optical imaging probe over a radio-imaging probe due to obvious inadequacies of the latter, including the requirement of sophisticated instruments and facilities, high costing with almost similar level of penetrations in the deep tissues [23].

During one of our initial *in silico* studies on the interactions of urea ligands with PSMA cavity [24], we have opined that incorporating a modified tyrosine unit in the targeting ligand may improve the binding

* Corresponding author at: Discipline of Chemistry, Indian Institute of Technology Indore, Khandwa Road, Simrol, Indore 453 552, Madhya Pradesh, India.
E-mail address: cvenkat@iiti.ac.in (V. Chelvam).

https://doi.org/10.1016/j.bioorg.2019.103154
Received 15 February 2019; Received in revised form 5 July 2019; Accepted 24 July 2019
Available online 30 July 2019

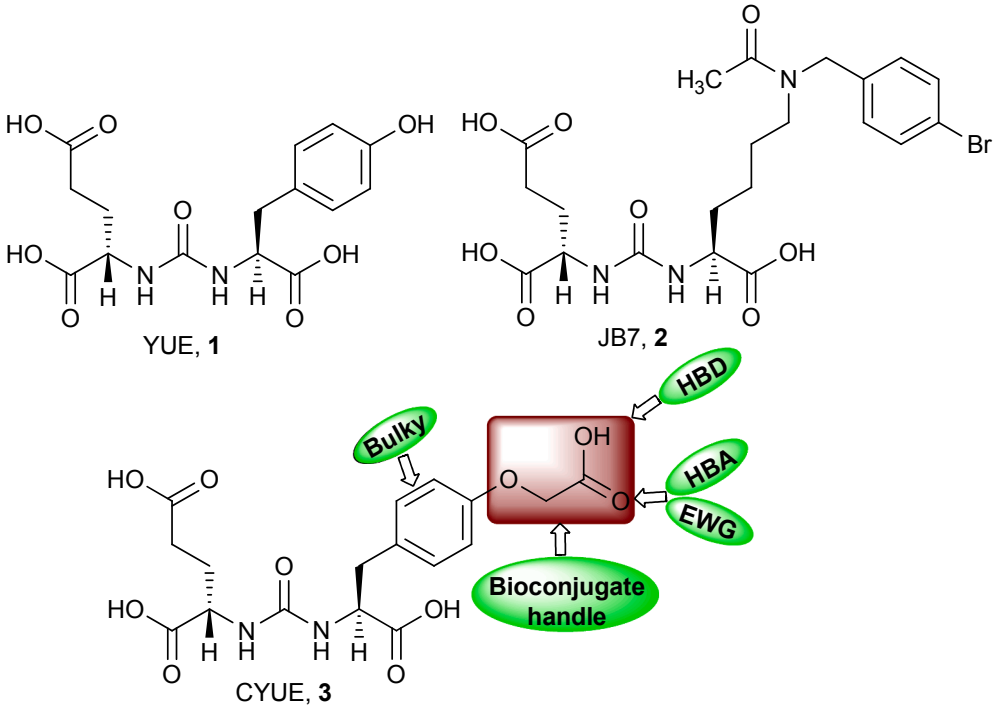

Fig. 1. Structure of PSMA inhibitors: Tyrosine glutamic acid-based urea ligand YUE, **1**; PSMA co-crystallized ligand JB7, **2** (PDB ID 4NGM); Carboxymethyl protected tyrosine glutamic acid-based urea ligand CYUE, **3**.

affinity. In the literature, the binding mode and modifications of Tyr-urea-Glu ligand was mostly unexplored except a reported radio-synthesis of [^{18}F]Et-Tyr-urea-Glu ligand devoid of any binding affinity and biological evaluation studies in PCa cells [25]. The phenolic –OH group of the tyrosine moiety provides an opportunity to design novel urea ligands with improved interactions in the S1 pocket and better binding affinity. The presence of phenyl ring improves hydrophobic interactions in the protein cavity, simultaneously, phenolic –OH can be modified into a bio-conjugate handle to attach peptidic spacer and a fluorescence tag. The enhanced chemical interactions of CYUE ligand with neighbouring amino acid residues in the active site of the PSMA increases the affinity and specificity of the ligand due to the presence of an additional hydrogen bond acceptor (carbonyl moiety of carboxylic group) and hydrogen bond donor functionality (−OH group of carboxylic acid moiety). The designed ligand was initially validated for improved binding interactions in the PSMA cavity via computational docking study and later synthesized to verify the hypothesis by biological evaluation in PSMA$^+$ and PSMA$^-$ cell lines.

Although many reports [26–28] have discussed unusual ligands for PSMA, only a few studies have focused on the structural modification of PSMA ligands by skilful analysis of the protein cavity. In this report, the novel PSMA ligand CYUE was rationally designed, chemically synthesized, and its fluorescent bio construct was systematically evaluated for diagnostic capacities *in vitro* in PSMA$^+$ and PSMA$^-$ cells.

2. Results and discussion

2.1. QSAR analysis

Recently, we have reported the structure-activity relationship (SAR) studies of urea-based molecules as potent PSMA inhibitors [24]. Using this SAR model, we have modified the glutamic acid-urea-tyrosine (YUE) inhibitor by introducing methylene carboxylic acid moiety through the phenolic hydroxy group. Through this critical alteration, we have introduced an electron withdrawing group in the form of carbonyl oxygen, a hydrogen bond donor in the form of –OH moiety of carboxylic acid (Fig. 1), well recommended from our SAR study. The newly designed inhibitor, CYUE, was analysed through QSAR, and the inhibitory constant was predicted (Table 1). The predicted K_i value of CYUE ligand was found to be better than its parent ligand (YUE).

2.2. Molecular docking analysis

It is well documented that in PSMA cavity, several amino acids present in S1 and S1′ pockets are crucial for better protein-ligand interactions. Moreover, the orientation of the amino acids and bimetallic zinc centres of PSMA determine the overall binding affinity of the ligand. Arg 210, Asn 257, Lys 699, Tyr 552, Tyr 700, Glu 424, and Glu 425 residues constitute the S1′ binding site in the protein and interact with the glutamic acid functionality of the urea ligand. The β15/ β16 hairpin bend with Lys 699 and Tyr 700 amino acid residues acts as a "glutarate sensor" [10] which is carefully preserved in designing new ligands for PSMA. Any modifications in this part of the ligand may be detrimental, resulting in loss of binding efficacy to PSMA. However, the S1 site of PSMA consisting of Gly 518, Asn 519, Arg 534, Arg 536 amino acid residues has considerable scope for modification of ligand architecture.

Keeping this in mind, a detailed docking study was performed on the designed urea ligand, CYUE. JB7, a urea-based inhibitor, co-crystallized with PSMA (PDB 4NGM) was selected from the protein data bank as a reference for performing the computational study. To validate the docking protocol, JB7 was re-docked in the active site of PSMA and RMSD value was calculated to be 1.09 Å with respect to its co-

Table 1
Prediction of PSMA inhibitory activity of CYUE (**3**) and YUE (**1**) ligands.

Ligands	Predicted PSMA inhibitory activity by QSAR model	
	pK_i	K_i (nM)
CYUE (**3**)	**7.2580**	55.21
YUE (**1**)	6.9566	110.51

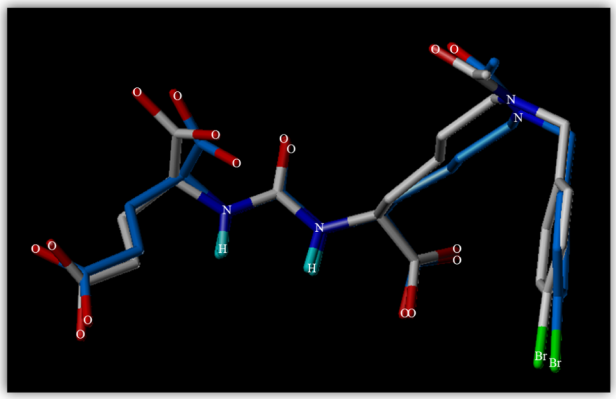

Fig. 2. Superimposed orientation of PSMA co-crystallised (PDB ID 4NGM) with ligand JB7; native (blue) and docked orientations (white).

crystallised orientation. The RMSD value was found to be less than the crystal resolution of 4NGM protein structure (1.84 Å) which suggests that the docking protocol is reliable. The similarity score of pre and post-docking poses of JB7, which is a crucial indicator for the validation of the protocol, was found to be 0.917 (Figs. 2 and 3).

After the validation, the same docking protocol was implemented for YUE and newly designed CYUE ligands to predict the probable interactions with the amino acid residues that might be responsible for PSMA inhibitory activity. According to the post-docking orientation of the three ligands (CYUE, YUE, JB7), glutamic acid moieties were superimposed on each other at the S1′ site of PSMA protein (Fig. 4). The α–carboxylic acid group of tyrosine amino acid in YUE (**1**) was positioned differently as compared to α–carboxylic acid of lysine in JB7. On the contrary, in CYUE (**3**), the orientation of α–carboxylic acid of modified tyrosine was perfectly aligned to the α–carboxylic acid of lysine in JB7.

Furthermore, urea moiety of YUE (**1**) was in a different alignment as compared to JB7 (Fig. 4), and the carbonyl oxygen of urea moiety is away from the catalytic Zn atoms of PSMA. For YUE (**1**), the distances between oxygen and zinc-1 or zinc-2 atoms were calculated to be 3.52 Å and 5.33 Å, respectively, which are much higher than the corresponding distances in the native orientation of JB7. After the strategic modification in YUE (**1**), the carbonyl oxygen of urea in CYUE (**3**) shifted towards the zinc atoms and the resultant distance between oxygen and zinc-1 or zinc-2 atoms reduced to 1.97 Å and 3.82 Å, respectively, resulting into a steep decline in the overall potential energy of the protein-ligand complex, and leading to an improvement in the binding affinity of CYUE (**3**) ligand. Additionally, the docking score of **3** was found to be 13.54, which was higher than for **1** (Table 2).

In the hydrogen bonding interaction analysis, at S1′ site, CYUE (**3**) interacts with six amino acid residues (Arg 210, Asn 257, Lys 699, Tyr 552, Tyr 700 and Glu 425) present in the protein cavity (Fig. 5) whereas YUE (**1**) interacts with only five of the amino acid residues at the S1′ site of PSMA (Fig. 6). Due to the strategic incorporation of carboxylic acid methylene spacer, CYUE (**3**) ligand has generated two new hydrogen bonding interactions with Asn 257 and Tyr 700 residues at the S1′ site. At the S1 site, due to the introduction of structural modification, a drastic change in the interaction of CYUE (**3**) is noticed. The CYUE (**3**) ligand generates five new hydrogen bonding interactions with the three new amino acid residues (Gly 518, Arg 536 and Asn 544). In summary, CYUE (**3**) interacts with twelve amino acid residues resulting in the formation of fifteen H-bonds, whereas YUE (**1**) interacts with only eight amino acid residues through thirteen H-bonds (Table 3). The enhanced interactions of CYUE (**3**) with a greater number of amino acids at PSMA active site has reflected in better docking score of **3** and improved binding affinity. The docking orientation and H-bonding interactions of CYUE (**3**) and YUE (**1**) with PSMA are depicted in Figs. 5 and 6, respectively.

Additionally, the H-bonding interactions of CYUE (**3**) and 2-[3-(1,3-dicarboxypropyl)ureido]pentanedioic acid (DUPA) ligands at the GCPII active site were also compared to understand the higher binding affinity of DUPA ligand reported in the literature. The H-bonding interactions of CYUE (**3**) and DUPA with the amino acid residues of PSMA cavity are

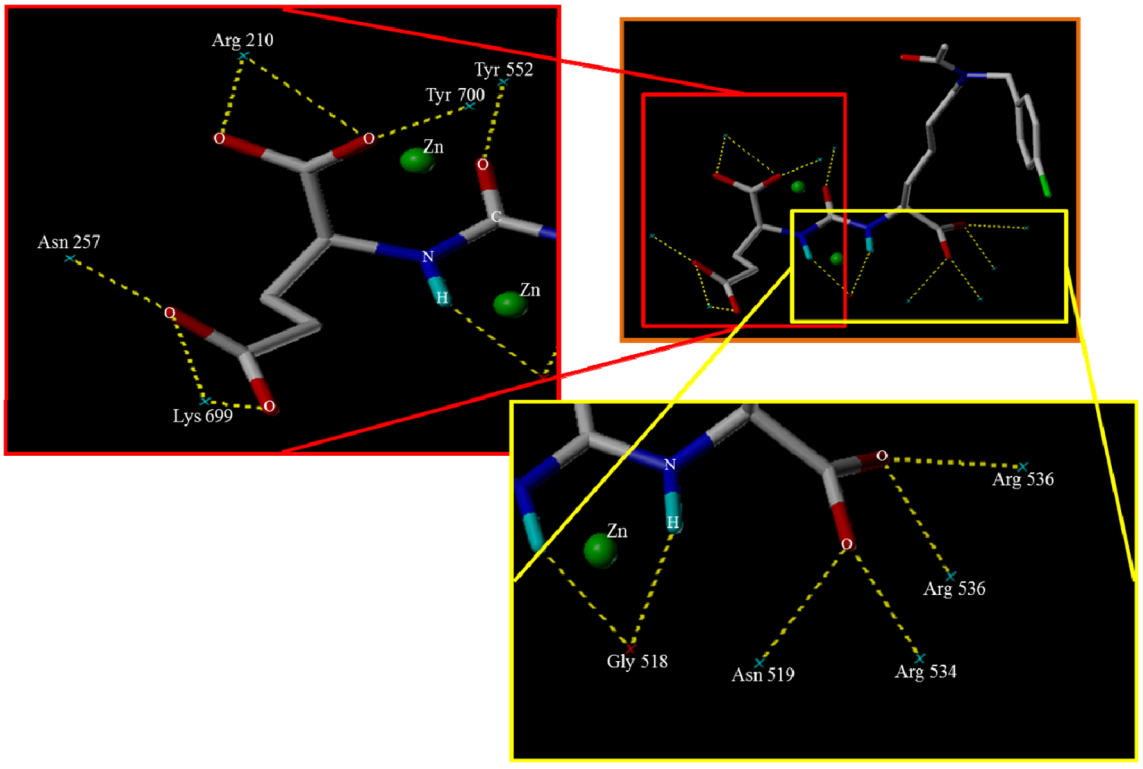

Fig. 3. Post docking hydrogen bonding interactions of JB7 in the cavity of PSMA protein (PDB ID 4NGM).

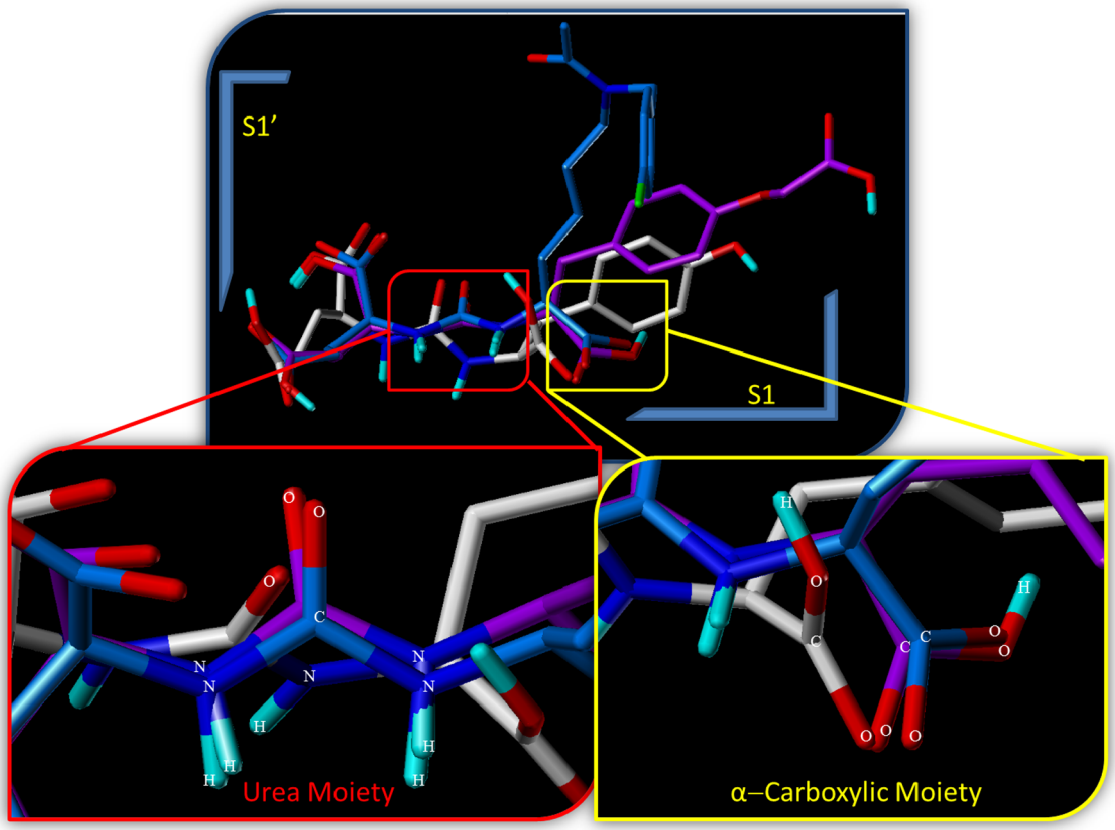

Fig. 4. Super-imposed docked poses of JB7 (blue), CYUE (**3**, purple) and YUE (**1**, white) ligands, at the active site of PSMA protein. S1′ and S1 are the sites present in the active cavity of PSMA protein. The urea moiety of the ligands **1–3** is mentioned within the red box and the α − carboxylic group in yellow box.

Table 2
Docking scores of ligands JB7, CYUE and YUE.

Ligands	Total Score	Similarity Score
JB7	16.46	0.917
CYUE (**3**)	13.54	0.545
YUE (**1**)	12.31	0.482

provided in the Table 4. The docking studies reveal that DUPA forms eight H-bonding interactions with six amino acid residues such as Arg 210, Asn257, Lys 699, Tyr 552, Tyr 700, Glu 245 at the S1' site whereas CYUE forms only seven H-bonding interactions. At S1 site of PSMA protein, DUPA forms ten H-bonding interactions with seven amino acid residues whereas CYUE forms only eight H-bonding interactions with six aminoacid residues.

We hypothesized that although CYUE has lesser number of interactions in the S1 pocket, TYR549 amino acid residue of PSMA active cavity might play a pivotal role in improving the binding affinity of CYUE ligand by providing hydrophobic interaction with the tyrosine moiety of the ligand.

After the aforementioned thorough analysis of docking and hydrogen bonding interactions of CYUE (**1**), we planned to conjugate CYUE (**3**) ligand to a fluorescent agent, rhodamine B, through a peptidic spacer for the development of a diagnostic tool, **16**, for imaging $PSMA^+$ cancers. We were curious to analyse the binding mode of **16** in the PSMA active site. The docking studies (Fig. 7) indicates that the H-bonding interactions of **16** are like that of the non-conjugated CYUE (**3**) ligand with additional H-bonding interactions with Arg 463 and Lys 514 residues of the protein. The superimposition of fluorescent conjugate **16** with JB7 clarifies that the conjugated CYUE (**3**) ligand is well aligned with the co-crystallised ligand (JB7) even with the bulky rhodamine B moiety attached which remains suspended outside the protein cavity and does not hamper the binding of **16** at the active site of PSMA (Fig. 8).

2.3. Chemical synthesis

The synthetic route to prepare the targeting ligand, CYUE (**3**) and fluorescent conjugate (**16**) are depicted in the Schemes 1 and 2. As outlined in Scheme 1, bis(*tert*-butyl)-*L*-glutamate **4** was treated with triphosgene in the presence of triethylamine to form an isocyanate intermediate **5**. *In situ* reaction of **5** with *L*-tyrosine *tert*-butyl ester **6** resulted in the formation of the tris(*tert*-butyl)carboxylic acid protected urea precursor **7**. To our delight, free phenolic hydroxyl present in *L*-tyrosine *tert*-butyl ester **6** doesn't compete with the reaction of **5** to form a carbamate. However, the amino group of **6** reacted exclusively with **5** to give **7** in an excellent yield of 90%. Further, the phenolic hydroxy group of **7** was alkylated with α-bromomethylacetate **8**, in the presence of Cs_2CO_3 in DMF at room temperature to provide **9** in moderate yield. The crucial step for regenerating the carboxylic acid group from **9**, required for solid phase peptide synthesis of bio-construct **16**, was carried out by the hydrolysis of the methyl ester **9** using trimethyltin hydroxide as a saponification agent. The methylester **9** was successfully hydrolyzed in a good yield of 76% to provide the required, tris(*tert*-butyl)carboxylic acid protected PSMA ligand precursor **10** (Scheme 1).

An elaborate solid phase peptide synthesis for the construction of required PSMA targeted fluorescent conjugate **16** is described in the Scheme 2. Solid phase peptide synthesis of **16** was performed using commercially available 1,2-diaminoethanetrityl resin **11**. The primary amino group present in **11** was coupled with Fmoc-Asp(O^tBu)–OH using PyBOP as a coupling agent to provide the dipeptide **12**. The NHFmoc amino group in the growing dipeptide chain **12** was deprotected using a solution of 20% piperidine in DMF. The Fmoc free amino group

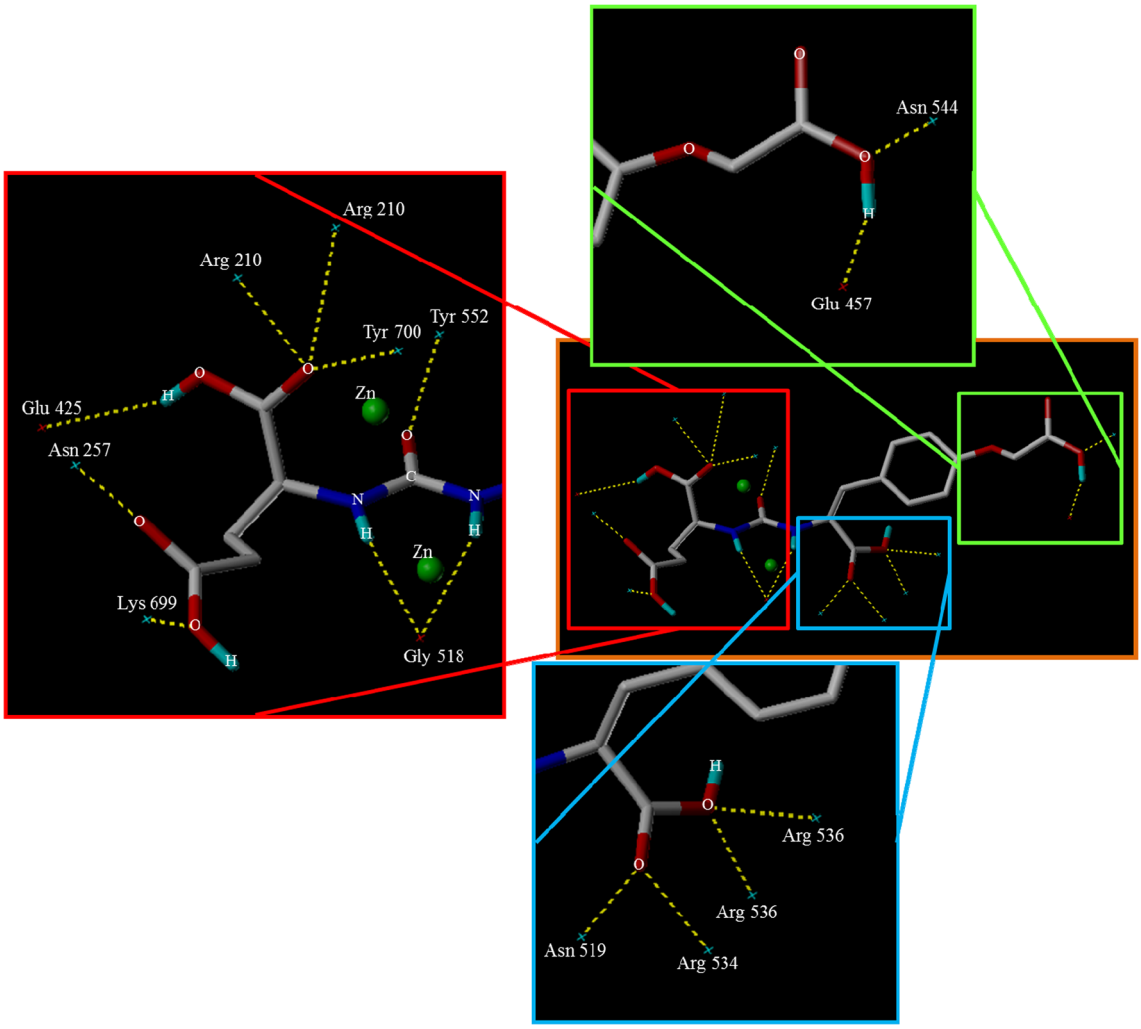

Fig. 5. Docking orientation and hydrogen bonding interactions of CYUE (**3**) ligand at the site of PSMA protein (PDB ID 4NGM).

generated from **12** was coupled with Fmoc-Lys(Tfa)–OH using standard coupling reagent to provide the growing tripeptide chain **13.** It is important to mention that the α-amino group of lysine protected as NHFmoc was labile to 20% piperidine in DMF and readily available for construction of next amide bond in the growing tripeptide chain whereas the ε-amino group of lysine protected as trifluoroacetyl group was stable under NHFmoc cleavage condition and it readily undergoes deprotection in 2M aqueous piperidine. The selection of α- and ε-amine protecting groups in the lysine amino acid, which are labile under different basic conditions, was crucial to our strategy of attaching a fluorescent agent to ε-amino group of lysine in the final step of the preparation of conjugate **16**. The NHFmoc amino group in the growing tripeptide chain **13** was deprotected using a solution of 20% piperidine in DMF. The Fmoc free amino group in **13** was now sequentially coupled with Fmoc-8-aminocaprylic acid, two molecules of Fmoc-Phe-OH and another molecule of Fmoc-8-aminocaprylic acid using standard amide coupling reagents to provide the growing heptapeptide chain **14**.

Addition of two molecules of 8-aminocaprylic acid to the peptide chain provides a 16-carbon atoms alkyl thread and ensures that the cargo of fluorescent agent is safely distanced away from the hydrophobic pocket along 20 Å deep tunnel present in the PSMA protein. In the peptidic spacer, the attachment of two phenylalanine moieties was essential and added to provide necessary hydrophobic interactions with the binding pocket present in 20 Å tunnel of the PSMA protein.[12] The amino group present in the NHFmoc protected heptapeptide chain **14** now awaits final attachment of tris(*tert*-butyl)carboxylic acid protected PSMA ligand precursor **10**. This was successfully achieved to provide the required trifluoroacetyl amino protected lysine polypeptide chain **15** and confirmed by observation of the negative Kaiser test. Having constructed the masked polypeptide chain **15**, the final step was deprotection of trifluoroacetyl protected ε-amino group of lysine using aqueous piperidine conditions to expose the free ε-amino group that can be tagged with a fluorescent agent, rhodamine B. The ε-amino trifluoroacetyl protecting group in **15** was deprotected successfully using 2M aqueous piperidine [29] and the fluorescent agent, rhodamine B was coupled using PyBOP as a coupling agent to give *t*-butylcarboxylic acid protected precursor of the final conjugate **16**.

The PSMA targeting rhodamine B conjugate **16** was released from the 1,2-diaminoethanetrityl resin, and simultaneously all the *tert*-butylcarboxylic acids are deprotected with the help of a cleaving cocktail TFA:TIS:H_2O (95:2.5:2.5). Excess trifluoroacetic acid was evaporated under reduced pressure using rotary evaporator, and the turbid pink viscous liquid is precipitated by the addition of ice-cold ether. The pink colored precipitate was washed thrice with ice-cold ether, centrifuged and dried under an inert atmosphere to provide the final PSMA targeting rhodamine B conjugate **16** that was purified using reverse phase HPLC.

2.4. In vitro studies

The selective uptake of the newly synthesized bio-construct **16** was evaluated by confocal laser scanning microscopy (CLSM) in LNCaP cells

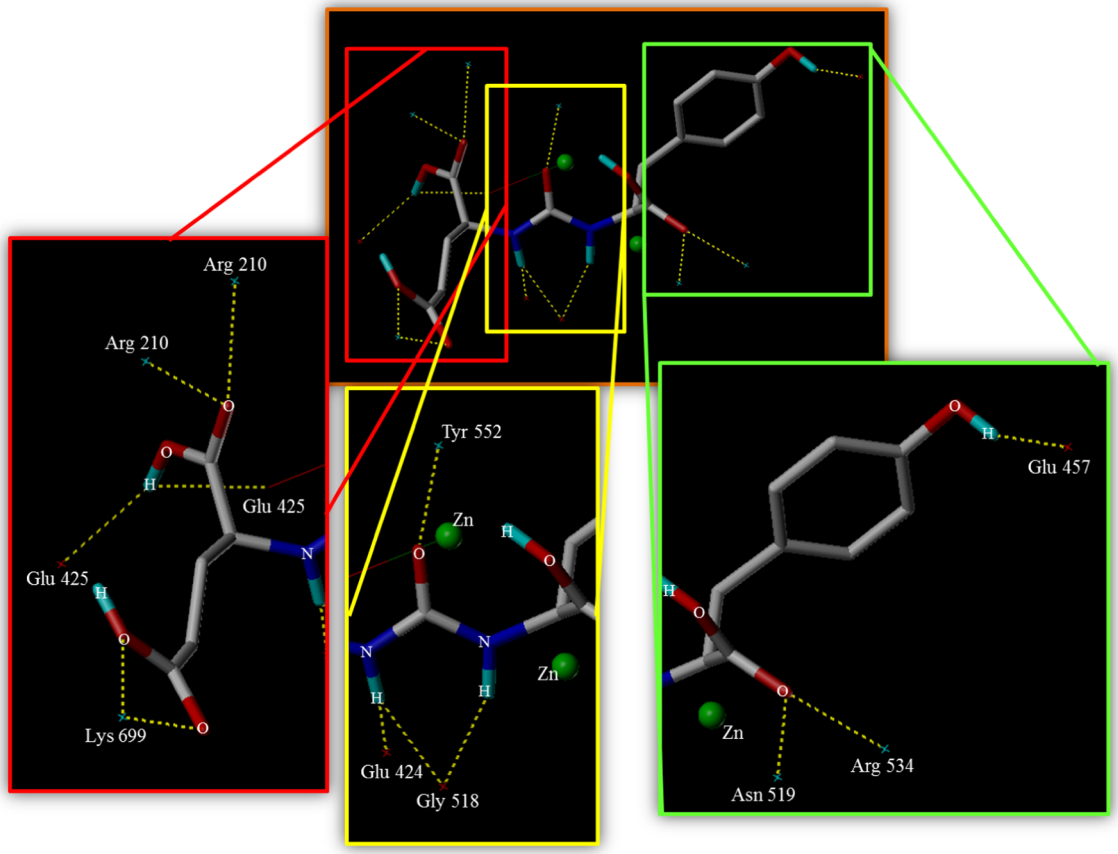

Fig. 6. Docking orientation and hydrogen bonding interactions of YUE (**1**) at the site of PSMA protein (PDB ID 4NGM).

(PSMA + ve) and PC-3 cells (PSMA –ve). LNCaP and PC-3 cells were incubated with four different concentrations of the fluorescent conjugate viz., 10, 25, 50 and 100 nM (See supporting information, Fig. S1). The fluorescence intensity in the cytoplasm of the LNCaP cells increases with the increase in the concentrations of **16**. The microscopic studies also reveal the distribution of the bio-construct **16** throughout the cytoplasm of $PSMA^+$ LNCaP cells. The lack of fluorescence signal in the PC-3 cells proves that the ligand conjugate **16** is protein specific. *In vitro* specificity of bioconjugate **16** was further examined by prior incubation of LNCaP cells with a 100-fold excess of a standard inhibitor, 2-PMPA. PSMA receptors blocked LNCaP cells display minimal uptake confirming the uptake of the bioconjugate **16** via receptor-mediated endocytosis and not through non-specific pathways (Fig. 9). Thus, we have successfully demonstrated that the fluorescent conjugate **16** traffic to the cytoplasm of the prostate cancer cells via PSMA mediated receptor endocytosis mechanism. The bio-construct **16** is highly target-specific, proving it to be an excellent potential candidate for delivery of payloads to cancer cells. The Lipinski rule of 5 is applicable only to small molecule ligands administered orally and not for the bioconjugate such as **16**, the molecular weight of which is higher (1733.85 g mol^{-1}) than the upper limit of small molecule drugs that are typically less than 500 g mol^{-1}. The conjugate **16** will be used to detect a disease by

Table 3
Comparative analysis of H-bonding interactions of JB7, CYUE (**3**) and YUE (**1**) ligands at the active site of PSMA (H-bond lengths are mentioned in Å).

Site	Amino Acid Residues	JB7- Natural Interactions	JB7 Post Docking Interactions	CYUE (3)	YUE (1)
S1′ site of PSMA	Arg 210	2.80	2.13, 2.41	2.69, 2.27	2.33, 1.95
	Asn 257	2.89	2.04	1.82	
	Lys 699	2.70	1.84, 2.62	1.79	1.97, 2.11
	Tyr 552	2.63	1.67	2.35	1.98
	Tyr 700	2.53	1.87	2.33	
	Glu 424	3.01			2.32, 2.01, 1.94
	Glu 425			2.41	2.19, 2.47
S1 site of PSMA	Gly 518	3.04, 3.05	2.13, 2.05	2.23, 2.37	
	Asn 519	2.98	2.51	1.86	1.90
	Arg 534	2.84	2.03	1.99	2.11
	Arg 536	2.99, 3.00	2.11, 2.40	2.04. 2.02	
	Glu 457			2.42	1.81
	Asn 544			1.91	
Distance between urea carbonyl oxygen and Zn-1 atom		2.57	2.66	1.97	3.52
Distance between urea carbonyl oxygen and Zn-2 atom		4.55	4.61	3.82	5.33

Table 4
Comparison of H-bonding interactions between CYUE (**3**) and *2-[3-(1,3-dicarboxypropyl)ureido]pentanedioic acid* (DUPA) ligands at the PSMA active site (H-bond lengths are mentioned in Å).

Site	Amino Acid Residues	CYUE (3)	DUPA
S1′ site of PSMA receptor	Arg 210	2.69, 2.27	1.86
	Asn 257	1.82	1.78, 2.7
	Lys 699	1.79	1.96
	Tyr 552	2.35	1.79
	Tyr 700	2.33	2.35, 1.87
	Glu 425	2.41	2.72
S1 site of PSMA receptor	Gly 518	2.23, 2.37	1.86
	Asn 519	1.86	2.07
	Arg 534	1.99	1.79, 2.57
	Arg 536	2.04. 2.02	2.53
	Glu 457	2.42	–
	Asn 544	1.91	–
	ASP387	–	2.69
	SER454	–	2.32, 2.40, 2.08
	TYR549	–	2.46

targeting biomarkers over-expressed on the surface of the diseased tissues by intravenous administration.

The binding affinity of CYUE fluorescent conjugate **16** on PSMA$^+$ cells was estimated by analysing uptake studies in LNCaP cells using Fluorescence Activated Cell Sorting (FACS) technique. The conjugate's ability to bind to PSMA is evaluated by measuring the mean fluorescence intensity per cell for different concentrations of the conjugate. A hyperbolic curve of different concentrations of the fluorescent inhibitor against the mean fluorescence intensity of **16** by PSMA$^+$ LNCaP cells yielded a dissociation constant K_D value of 88 nM (Fig. 10). The curve shows a slow exponential increase in the uptake of the fluorescent conjugate **16** targeted to the PSMA receptor followed by saturation of the curve for concentrations higher than 200 nM due to full occupancy of PSMA receptors present in the LNCaP cells with the conjugate **16**. The low dissociation constant value (< 100 nM) gives indisputable evidence of the high affinity of the ligand-peptide spacer to the PSMA protein and its perfect fit inside the protein tunnel. The PSMA receptors were blocked completely by using 100-fold excess PMPA, indicating that the CYUE fluorescent conjugate **16** undergoes internalisation via receptor-mediated endocytosis and not through non-specific means into the LNCaP cells.

The introduction of tyrosine moiety in the ligand conjugate **16** was expected to increase the affinity drastically in the binding pocket of PSMA but the binding affinity of the conjugate **16** (K_D = 88 nM) was significantly lower compared to DUPA ligand (K_D = 8 nM). This is because, from the analysis of Table 4, it was found that DUPA has two extra number of H-bonding interactions compared to CYUE (**3**) ligand. The lower binding affinity of CYUE (**3**) could be improved by adding more hydrophobic moieties in addition to two phenylalanine moieties used in the current spacer of the bioconjugate **16** that interacts with the 20 Å tunnel of PSMA protein. A remote arene-binding site on PSMA was discovered few years ago [30] and proven to enhance the binding affinity of the bioconjugates used for recruiting antibody to target and destroy prostate cancer cells. The arene binding site of PSMA is proposed to interact strongly with 2,4-dinitrophenylamine moiety present in the bioconjugate spacer of antibody recruiting molecules. Therefore, introduction of an additional arene moiety in the spacer may help to enhance the binding affinity of biconjugate **16** which is currently under investigation.

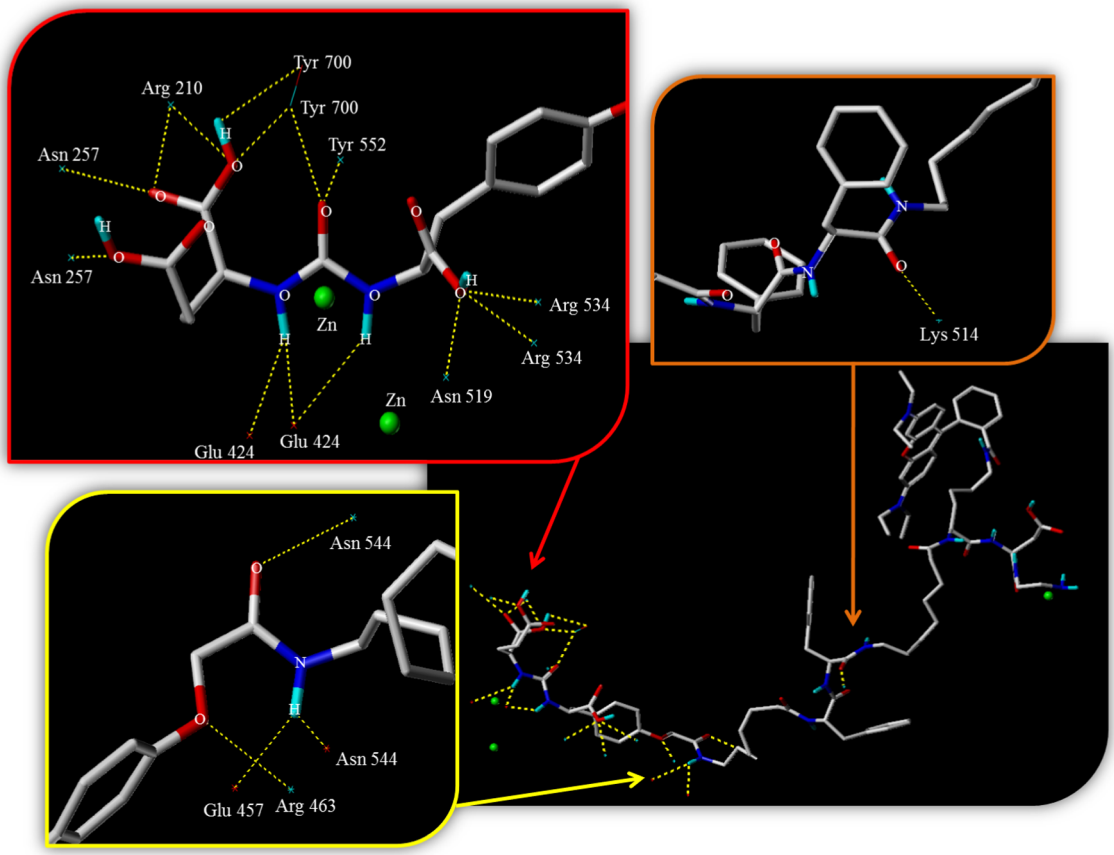

Fig. 7. Docking orientation and hydrogen bonding interactions of CYUE-Rhodamine B conjugate (**16**) at the site of PSMA protein (PDB ID 4NGM).

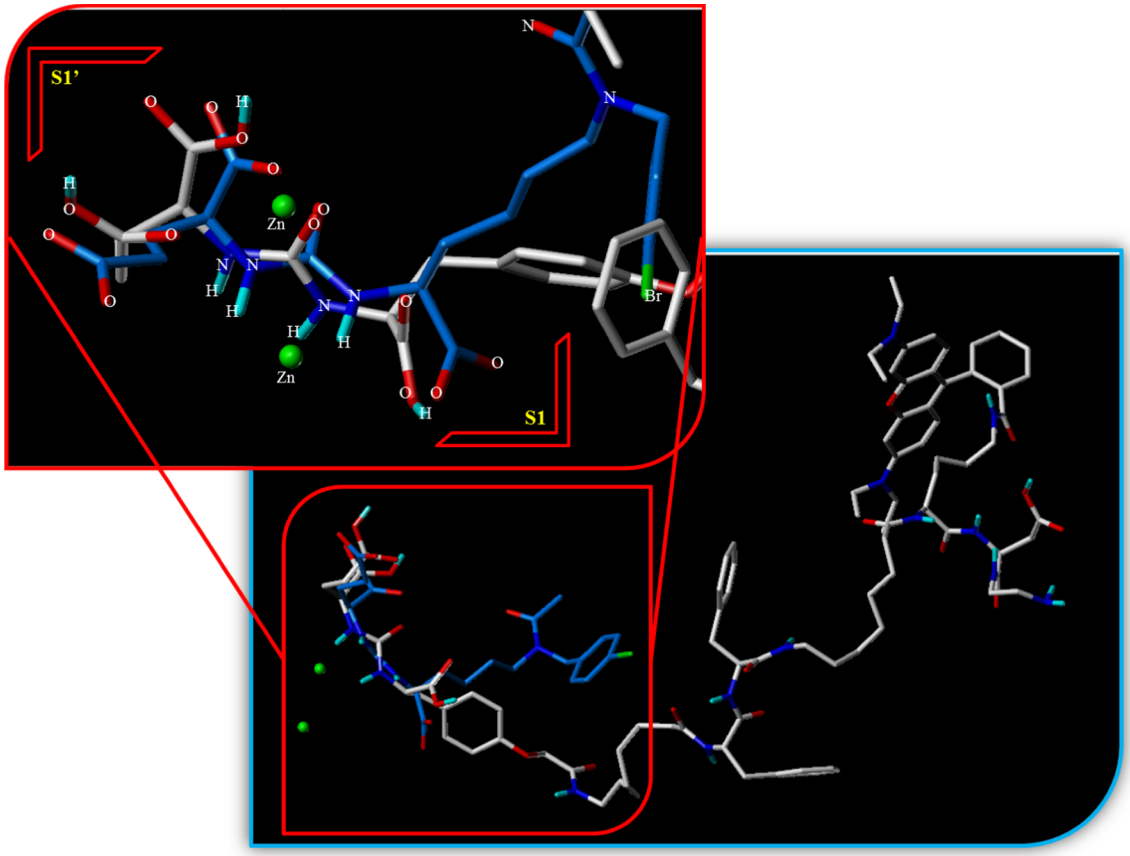

Fig. 8. Superimposed docked orientations of CYUE-Rhodamine conjugate (**16**, white) and JB7 (blue).

3. Conclusion

In summary, we have developed a novel tyrosine-based asymmetric urea ligand (CYUE) for targeting PSMA$^+$ cancers based on a comprehensive SAR studies established from our research findings. Through docking studies, a reasonable explanation was provided for the improved binding affinity of the new PSMA ligand. Further, CYUE ligand was chemically synthesized and transformed into a fluorescent labelled oligopeptide bio-construct to target PSMA$^+$ cancers. Successful *in vitro* application by targeted delivery and binding affinity measurement studies have set the platform for future *in vivo* studies and clinical use of the bio-construct as an imaging agent for detection of deeply seated tumour tissues during intraoperative surgery.

4. Experimental section

4.1. Molecular docking study

The crystal structure of the target protein Glutamate carboxypeptidase II (PDB ID 4NGM) was retrieved from the protein data bank. In 4NGM, PSMA was co-crystallised with a urea-based ligand JB7, which is structurally very close to the designed CYUE (**3**) ligand.

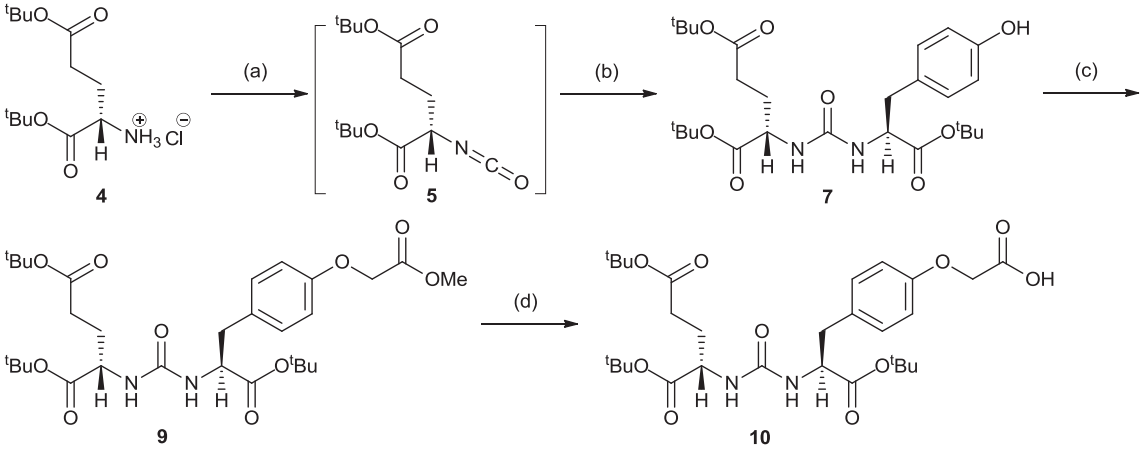

Scheme 1. Reagents and conditions: (a) Triphosgene, triethylamine, dichloromethane (CH_2Cl_2), −50 °C to rt; (b) L-tyrosine *tert*-butyl ester (**6**), triethylamine, dichloromethane (CH_2Cl_2), rt, overnight; (c) α-Bromomethylacetate (**8**), Cs_2CO_3, *N,N*-dimethyl formamide (DMF), rt, 4 h; (d) Me_3SnOH, 1,2-dichloroethane (DCE), 80 °C, 4 h.

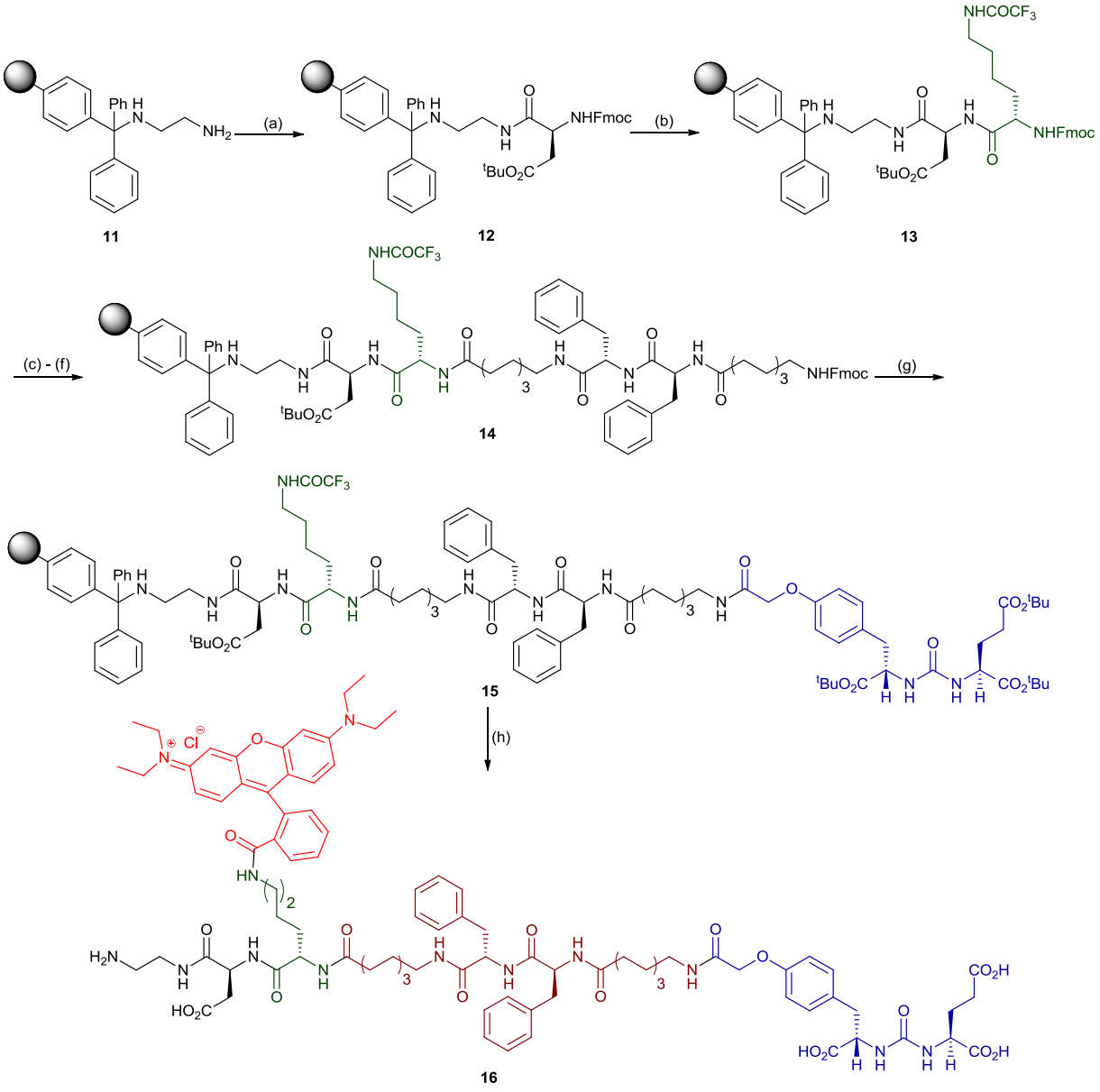

Scheme 2. Reagents and conditions: (a) Fmoc-Asp(O^{t}Bu)–OH, PyBOP, DIPEA, DMF, 6 h; (b) (i) 20% piperidine in DMF, rt, 30 min; (ii) Fmoc-Lys(Tfa)–OH, PyBOP, DIPEA, DMF, 6 h; (c) (i) 20% piperidine in DMF, rt, 30 min; (ii) Fmoc-8-aminocaprylic acid, PyBOP, DIPEA, DMF, 6 h; (d) (i) 20% piperidine in DMF, rt, 30 min; (ii) Fmoc-Phe-OH, PyBOP, DIPEA, DMF, 6 h; (e) (i) 20% piperidine in DMF, rt, 30 min; (ii) Fmoc-Phe-OH, PyBOP, DIPEA, DMF, 6 h; (f) (i) 20% piperidine in DMF, rt, 30 min; (ii) Fmoc-8-aminocaprylic acid, PyBOP, DIPEA, DMF, 6 h; (g) (i) 20% piperidine in DMF, rt, 30 min; (ii) CYUE(^{t}BuO)$_3$-OH, PyBOP, DIPEA, DMF, 6 h; (h) (i) 2 M piperidine in water, rt, 6–12 h; (ii) Rhodamine B, PyBOP, DIPEA, DMF, 6 h; (iii) TFA:TIS:H_2O (95:2.5:2.5) (1 × 5 mL, 30 min; 2 × 2.5 mL, 15 min); (iv) Evaporate TFA; (v) Precipitate in ice-cold diethylether.

Docking studies were performed by the Surflex Dock method using Sybyl X 2.1.1 software.

All the water molecules were removed from 4NGM, and the missing hydrogen atoms were added. Force field AMBER7FF99 was applied to minimize the energy of the protein. A protomol was generated at the active site of protein and CYUE (**3**), YUE (**1**) and JB7 ligands were docked into the PSMA cavity to check their respective interactions with the protein by using the same protocol. Later, to obtain an insight into the binding interactions of CYUE-Rhodamine B conjugate **16** with PSMA protein, bigger protomol was generated and the docking study was performed by keeping all the other *in silico* parameters constant.

RMSD values were calculated for co-crystallised JB7 and re-docked JB7 by importing docking outputs files in Discovery studio 4.0. RMSD values lesser than 2 Å are generally considered as an indicator of docking protocol validity.

The Surflex docking module of software Sybyl uses a similarity score (ranging from −1 to +1) to compare the orientation of newly designed ligand with the reference ligand, and +1 is considered as ideal match according to the orientation of ligand in the protein cavity.

4.2. Synthesis

4.2.1. General methods and materials

1,2-Diaminoethanetrityl resin, Fmoc-amino acids, coupling reagents and solvents used in the solid phase peptide synthesis (SPPS) as well as in the chemical synthesis were purchased from Iris Biotech GmbH, Sigma Aldrich, Merck and Spectrochem. Various dry solvents were prepared by using appropriate drying agents and standard procedures. Moisture and oxygen sensitive reactions were carried out under nitrogen atmosphere. Thin layer chromatography (TLC) was performed

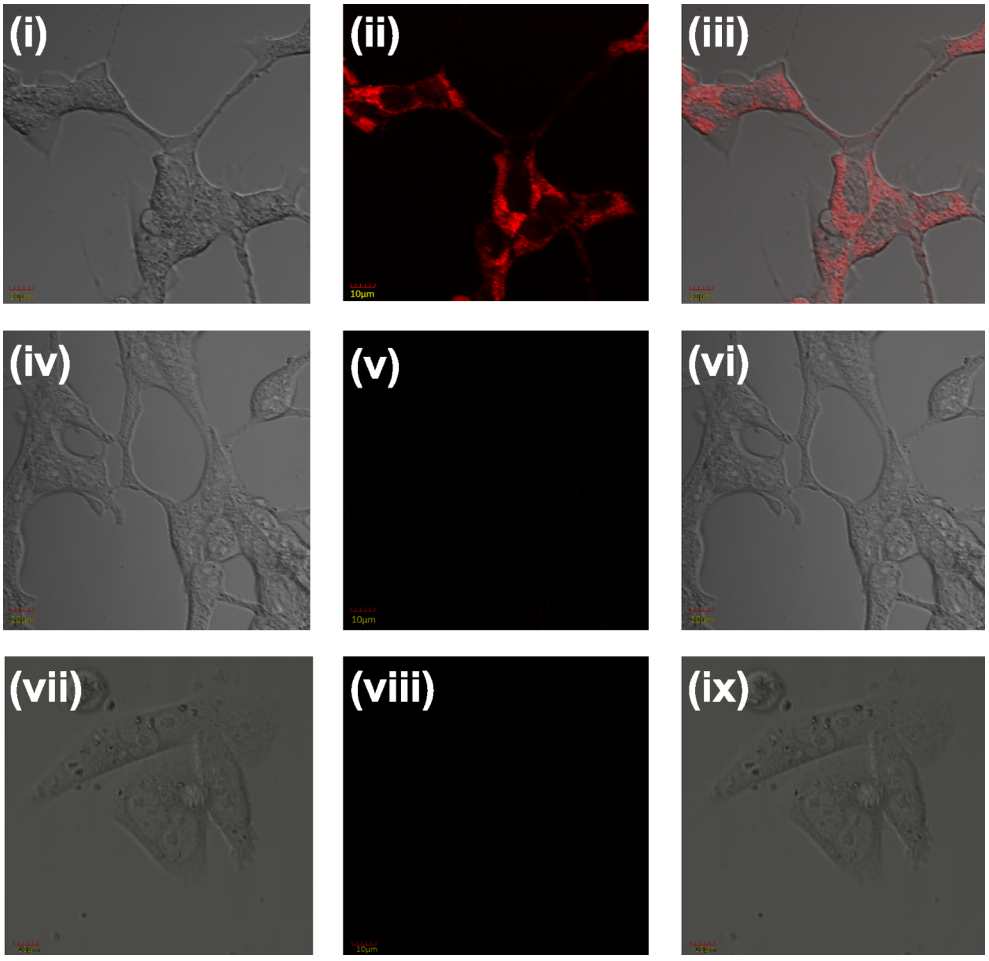

Fig. 9. (i) and (iv) DIC images of LNCaP cells ($PSMA^+$), (ii) Binding and internalization of CYUE rhodamine B conjugate **16** in LNCaP cells ($PSMA^+$) at 100 nM concentration, (iii) Overlay of (i) and (ii) to show that the uptake of **16** is in the cytoplasm of LNCaP cells, (v) Binding and internalization of **16** in the presence of 100-fold excess of 2-PMPA to block the PSMA receptors, (vi) Overlay of (iv) and (v) showing negligible uptake of CYUE rhodamine B conjugate, (vii) DIC image of PC-3 cells ($PSMA^-$), (viii) Specificity of CYUE rhodamine B conjugate in PC-3 cells ($PSMA^-$), (ix) Overlay of (vii) and (viii).

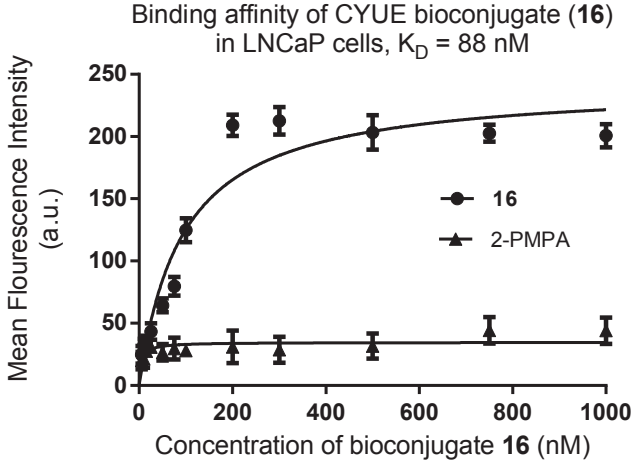

Fig. 10. Binding affinity (•) and competition or blocking studies (▲) of CYUE-Rhodamine conjugate **16** in $PSMA^+$ LNCaP cells over a range of concentrations plotted against the mean fluorescence intensity.

on silica gel glass TLC plates (60 F_{254}) and visualized under UV light to monitor the progress of the reaction. All compounds were purified by column chromatography using 100–200 or 230–400 mesh silica-gel as the stationary phase. Distilled hexane and ethyl acetate were used as eluents in the column chromatography.

Peptide synthesis was performed manually by using peptide vessels (Chemglass) and standard peptide coupling procedures. ^1H and ^{13}C NMR spectra were recorded using Bruker AV 400 MHz NMR spectrometer with TMS as an internal standard. ^1H NMR signals were reported in ppm with reference to residual $CHCl_3$ (7.25 ppm) and multiplicity was reported as s = singlet, d = doublet, t = triplet, q = quartet, m = multiplet or unresolved, and brs = broad singlet, with coupling constants in Hz. $CDCl_3$ was used as the solvent for recording NMR spectra. Mass spectra were recorded on Bruker micro TOF-Q II instrument using positive or negative mode electrospray ionization methods.

The purity of CYUE-Rhodamine B peptide conjugate **16** was analyzed using Dionex HPLC-Ultimate 3000 Analytical HPLC instrument. The peptide conjugate **16** was purified using RP-PFP column (XSelect CSH Prep Fluorophenyl 5 μm OBD, 19 mm × 150 mm) in Buchi Reveleris High Performance Preparative Chromatography instrument.

4.2.2. Synthesis of PSMA ligand precursor 10

4.2.2.1. Synthesis of (S)-di-tert-butyl 2-(3-((S)-1-(tert-butoxy)-3-(4-hydroxyphenyl)-1-oxopropan-2-yl)ureido)pentane dioate (7). Triphosgene (0.100 g, 0.33 mmol) was dissolved in dry dichloromethane (5 mL) and the solution was stirred at −50 °C under an inert atmosphere in a double-neck round-bottom flask (50 mL). Bis(*tert*-butyl)-*L*-glutamate hydrochloride salt **4** (0.296 g, 1.00 mmol) dissolved dry DCM (2 mL) was added to the triphosgene solution at −50 °C and triethylamine (0.460 mL, 3.3 mmol) was added dropwise to the reaction mixture. The reaction mixture was stirred for 1.5 h at −50 °C and stirred for another 1.5 h at room

temperature for the generation of isocyanate intermediate **5**. Thereafter, a solution of L-tyrosine-*tert*-butyl ester **6** (0.237 g, 1.0 mmol) and triethylamine (0.1 mL, 0.66 mmol) in dry DCM (2 mL) was added to the reaction mixture and the progress of reaction was monitored through TLC using ethyl acetate and hexane (1:2) mixture as eluent. The reaction mixture was further stirred for overnight at room temperature. After the completion of the reaction, the reaction mixture was concentrated under reduced pressure, diluted with ethyl acetate (25 mL), washed with water (2 × 10 mL) and brine (2 × 10 mL). The organic layer was dried over anhydrous Na_2SO_4, filtered and the solvent was evaporated under reduced pressure to afford the crude reaction mixture which was purified by column chromatography over 100–200 mesh silica gel using 25–30% ethyl acetate and hexane as eluent. The purified compound **7** was obtained as a colourless viscous liquid which gradually solidified to white solid; Yield 90% (0.469 g); R_f = 0.4 (EtOAc: hexane = 1:2); IR (CH_2Cl_2) 3366 (O—H), 3123 (N—H), 2979 (=C—H), 2932 (C—H), 1732 (C=O), 1642 (N—H), 1557 (C=C), 1455 (C—H), 1155 (C—O), 751, 698 (=C—H) cm^{-1}; ^1H NMR ($CDCl_3$, 400 MHz) δ 6.97 (d, J = 7.80 Hz, 2H), 6.69 (d, J = 7.80 Hz, 2H), 6.44 (brs, 1H) 5.18 (d, J = 7.52 Hz, 1H), 5.06 (d, J = 7.52 Hz, 1H), 4.62–4.47 (m, 1H), 4.38–4.25 (m, 1H), 2.98–2.91 (m, 2H), 2.35–2.15 (m, 2H), 2.10–1.94 (m, 1H) 1.83–1.69 (m, 1H), 1.44 (s, 9H), 1.41 (s, 18H); ^{13}C NMR ($CDCl_3$, 100 MHz) δ 172.6, 172.5, 171.7, 156.9, 155.4, 130.6, 127.5, 115.5, 82.3, 82.1, 80.7, 54.7, 52.9, 37.7, 31.6, 28.3, 28.05, 28.0; HRMS (ESI) m/z calcd for $C_{27}H_{42}N_2O_8$ $[M + Na]^+$ 545.2833, found 545.2734.

4.2.2.2. Synthesis of (S)-di-tert-butyl-2-(3-((S)-1-(tert-butoxy)-3-(4-(2-methoxy-2-oxoethoxy)phenyl)-1-oxopropan-2-yl)ureido)pentanedioate (9). Compound **7** (0.400 g, 0.77 mmol) and Cs_2CO_3 (0.375 g, 1.15 mmol) were suspended in freshly distilled dry DMF (5 mL) in a round-bottom flask (50 mL) and the resulting mixture was stirred for 30 min at room temperature. α-Bromomethylacetate **8** (0.17 mL, 1.53 mmol) was added to the reaction mixture and the reaction progress was monitored by TLC using ethyl acetate and hexane as eluent. The reaction was continued for 4 h until all the starting material was consumed and quenched immediately to avoid side product formation by adding brine solution (15 mL) followed by ethyl acetate (25 mL). The organic layer was extracted with ethyl acetate (2 × 25 mL) and dried over anhydrous Na_2SO_4. The solvent was filtered, concentrated under reduced pressure using rotary evaporator. The crude reaction mixture was purified through column chromatography using 100–200 mesh silica gel using 25% ethyl acetate-hexane mixture as eluent. The pure compound **9** was obtained as colourless viscous liquid which solidified on standing; Yield 89% (0.409 g); R_f = 0.42 (EtOAc: hexane = 1:2); IR (CH_2Cl_2) 3341 (N—H), 2979 (=C—H), 2932 (C—H), 1732 (C=O), 1657 (N—H), 1517 (C=C), 1455 (C—H), 1155 (C—O), 748, 698 (=C—H) cm^{-1}. ^1H NMR ($CDCl_3$, 400 MHz) δ 7.08 (d, J = 8.28 Hz, 2H), 6.81 (d, J = 8.28 Hz, 2H), 4.95 (d, J = 7.80 Hz, 1H), 4.87 (d, J = 7.80 Hz, 1H), 4.59 (s, 2H), 4.58–4.52 (m, 1H), 4.76 (ddd, J = 6.26, 5.50, 5.00 Hz, 1H), 3.79 (s, 3H), 3.02 (dd, J = 14.04, 5.24 Hz, 1H), 2.96 (dd, J = 14.04, 6.28 Hz, 1H), 2.40–2.15 (m, 2H), 2.12–1.98 (m, 1H), 1.89–1.76 (m, 1H), 1.46 (s, 9H); 1.41 (s, 9H), 1.38 (s, 9H); ^{13}C NMR ($CDCl_3$, 100 MHz) δ 171.4, 171.0, 170.3, 168.4, 155.7, 155.40, 129.8, 128.7, 113.5, 81.04, 81.01, 79.5, 64.4, 53.5, 52.0, 51.2, 36.8, 30.6, 27.3, 27.0, 26.99, 26.96; HRMS (ESI) m/z calcd for $C_{30}H_{46}N_2O_{10}$ $[M + Na]^+$ 617.3045, found 617.2944.

4.2.2.3. Synthesis of 2-(4-((S)-3-(tert-butoxy)-2-(3-((S)-1,5-di-tert-butoxy-1,5-dioxopentan-2-yl)ureido)-3-oxopropyl) phenoxy)acetic acid (10). A mixture of **9** (0.235 g, 0.40 mmol), Me_3SnOH (0.215 g, 1.19 mmol) and dry 1,2-dicloroethane (5 mL) were taken in a single neck round-bottom flask (25 mL). A reflux condenser was fitted with the round bottom flask and the reaction mixture was heated at 80 °C in an oil bath for 4 h. The reaction progress was monitored by TLC. After 4 h, the reaction mixture was concentrated under reduced pressure, diluted with ethyl acetate (25 mL) and washed with 0.1 N $KHSO_4$ solution (15 mL). The organic layer was extracted with ethyl acetate (2 × 25 mL), dried over anhydrous Na_2SO_4, filtered and then concentrated under reduced pressure. The crude reaction mixture was purified through column chromatography using 100–200 mesh silica gel using 75% ethyl acetate and hexane as eluent. The pure product of **10** was obtained as colourless viscous liquid; Yield 76% (0.172 g); R_f = 0.23 (EtOAc); IR (CH_2Cl_2) 3414 (O—H), 3357, 3124 (N—H), 2980 (=C—H), 2936 (C—H), 1731, 1707 (C=O), 1638 (N—H), 1545 (C=C), 1458 (C—H), 1158 (C—O), 750, 657 (=C—H) cm^{-1}. ^1H NMR ($CDCl_3$, 400 MHz) δ 7.04 (d, J = 7.52 Hz, 2H), 6.78 (d, J = 7.52 Hz, 2H), 5.55 (brs, 1H), 5.36 (brs, 1H), 4.70–4.20 (m, 4H), 2.97 (s, 2H), 2.35–2.15 (m, 2H), 2.10–1.95 (m, 1H), 1.87–1.72 (m, 1H), 1.45 (s, 9H), 1.41 (s, 18H); ^{13}C NMR ($CDCl_3$, 100 MHz) δ 172.7, 172.6, 172.5, 171.7, 157.1, 156.6, 130.8, 129.4, 114.5, 82.3, 82.1, 80.6, 65.4, 54.6, 52.9, 37.6, 31.6, 28.3, 28.1, 27.9*; HRMS (ESI) m/z calcd for $C_{29}H_{44}N_2O_{10}$ $[M + Na]^+$ 603.2888, found 603.2792. *higher intensity carbon

4.2.3. Synthesis of fluorescent labeled CYUE bio-conjugate 16

4.2.3.1. Resin swelling. All the resins used in solid phase peptide synthesis were swelled initially with DCM (5 mL) for 30 min by bubbling nitrogen and after draining DCM, the resin is swelled again with DMF (3 × 5 mL) for 15 min each.

4.2.3.2. General procedure for the Kaiser test. Few resin beads were taken in a test-tube and 2 drops of each of ninhydrin, phenol and 0.1% potassium cyanide solution were added to the test-tube and heated for 2 min at 110 °C in a sand bath. The presence of free amine group was confirmed by the appearance of dark blue colored resin beads in the test tube. The test was conducted after performing coupling of each amino acids following the aforementioned procedure.

4.2.3.3. General procedure for NHFmoc deprotection. The Fmoc-amino group in the growing peptide chain was deprotected in each step using 20% piperidine in DMF (10 mL) by bubbling nitrogen for 10 min through the swelled resin beads. The procedure was repeated thrice (1 × 4 mL; 2 × 3 mL) to ensure complete deprotection of Fmoc protecting group.

4.2.3.4. Typical solid phase peptide synthesis (SPPS) procedure. 1,2-Diaminoethanetrityl resin (0.050 g, 0.06 mmol) was initially swelled in DCM (5 mL) followed by DMF (5 mL). *N*-Fmoc-Asp(O^{t}Bu)–OH (0.061 g, 0.15 mmol), PyBOP (0.078 g, 0.15 mmol) and DIPEA (0.10 mL, 0.60 mmol) in 0.5 mL DMF was added to the peptide vessel containing resin beads and the coupling reaction was continued for 6 h. The resin beads were washed with DMF (3 × 3 mL) followed by washing with isopropanol (3 × 3 mL). Completion of peptide coupling reaction was confirmed by performing the Kaiser test (KT). Then a solution of 20% piperidine in DMF (1 × 4 mL; 2 × 3 mL) was added to the peptide vessel to cleave NHFmoc protecting group. Resin beads were washed with DMF (3 × 3 mL) followed by isopropanol (3 × 3 mL) and the formation of free amine was confirmed by the Kaiser test. A series of amino acids such as Fmoc-Lys(Tfa)–OH (0.070 g, 0.15 mmol), Fmoc-8-aminocaprylic acid (0.057 g, 0.15 mmol), Fmoc-Phe-OH (0.058 g, 0.15 mmol), Fmoc-Phe-OH (0.058 g, 0.15 mmol) and Fmoc-8-aminocaprylic acid (0.057 g, 0.15 mmol) were coupled to the growing peptide chain in a similar way as mentioned before. After the deprotection of Fmoc group from the last amino acid, Fmoc-8-aminocaprylic acid, tris-*tert*-butylcarboxylic protected CYUE precursor **10** (0.052 g, 0.09 mmol), PyBOP (0.078 g, 0.15 mmol) and DIPEA (0.10 mL, 0.6 mmol) in 0.5 mL DMF was added to the vessel and reacted for 6 h. The completion of reaction was again confirmed by the Kaiser test. Finally, the trifluoroacetyl group of lysine was cleaved by 6–12 h treatment with 2M aqueous piperidine at room temperature and the complete deprotection of Tfa was confirmed by the Kaiser test. Rhodamine B dye (0.043 g, 0.09 mmol), PyBOP (0.078 g, 0.15 mmol) and DIPEA (0.01 mL, 0.6 mmol) in 0.5 mL DMF was added to the peptide vessel and swelled for 6 h at room temperature. The completion

of rhodamine B coupling reaction was confirmed by the Kaiser test.

4.2.3.5. General procedure for peptide cleavage from resin beads. A mixture of 9.5 mL trifluoroacetic acid (TFA), 0.25 mL triisopropylsilane (TIPS), and 0.25 mL H_2O was prepared, and 5 mL of this cocktail solution was added to resin beads and nitrogen was bubbled through the solution for 30 min. Same procedure was repeated twice using 2.5 mL (15 min each) of cocktail solution. The collected mother liquor from cleavage was evaporated under reduced pressure and the concentrated viscous liquid was precipitated in ice cold diethyl ether. The precipitated product was dried under nitrogen atmosphere, the crude product was purified through HPLC.

4.2.4. Analytical HPLC method

The purity of bio-conjugate **16** was analyzed using a Dionex HPLC-Ultimate 3000 system. Typically a solution of bio-conjugate **16** (20 μL, 1.0 mg/1.0 mL) in a mixture of CH_3CN:H_2O (1: 1) was injected via autosampler and eluted using Dionex Acclaim ® 120 C_{18}, 5 μm, 4.6 mm × 250 mm analytical column at a flow rate of 1 mL/min (mobile phase, A = 0.1% trifluoro acetic acid/H_2O and B = acetonitrile). An isocratic flow of 40% B (v/v) was used during the run for 0 to 4 min and gradually gradient of B was increased to 100% B (v/v) over a period of 40-min. The chromatogram of **16** was recorded on the Ultimate 3000 RS variable wavelength detector at 225–280 nm with t_R = 19.5 min.

4.2.5. Preparative HPLC method

The purification of bioconjugate **16** was performed using Buchi Reveleris Prep HPLC System. Crude bioconjugate **16** (20 mg) was dissolved in 1:1 ratio of CH_3CN:H_2O (1 mL) and injected into the sample injector for elution using RP-PFP (Reverse Phase PentafluoroPhenyl) preparative column (XSelect CSH Prep Fluorophenyl 5 μm OBD, 19 mm × 150 mm). A flow rate of 10 mL/min (mobile phase, A = 0.1% trifluoro acetic acid/H_2O and B = acetonitrile) is maintained throughout the run and the mobile phase gradient was increased from 1% B (v/v) to 50% B (v/v) over a period of 40 min. The mobile phase gradient was further increased to 80% B (v/v) in the next 15 min and the chromatogram was recorded at λ = 280 or 555 nm. Pure fractions of **16** were collected using automatic fraction collector, acetonitrile was evaporated under reduced pressure and after lyophilization pure bioconjugate **16** was obtained. HRMS (+ESI) calcd for $[M-Cl]^+$ $(C_{91}H_{120}N_{13}O_{19})^+$ 1698.8818 found 1698.8807.

4.3. In vitro studies

4.3.1. Culturing of cell lines

LNCaP and PC-3 cell lines were purchased from National Centre for Cell Science (NCCS), Pune, India. The cell lines were grown as a monolayer until confluent in sterile filtered RPMI 1640 medium supplemented with 10% heat inactivated fetal bovine serum (HIFBS), 1% Penicillin-Streptomycin antibiotic and 100 mM of sodium pyruvate in 5% CO_2:95% air humidified atmosphere, at 37 °C.

4.3.2. Confocal laser scanning microscopy (CLSM) studies

LNCaP (50,000 cells/well in 0.5 mL medium) and PC-3 (25,000 cells/well in 0.5 mL medium) cells were trypsinized and seeded into Nunc Lab Tek II Chambered Coverglass System for 72 h and 48 h respectively. The spent medium was replaced with increasing concentrations (10, 25, 50, 100 nM) of **16** prepared in medium (0.5 mL) and incubated at 37 °C for 1 h. For competition experiment, LNCaP cells were incubated at 37 °C with 100–fold excess concentration of 2-PMPA prior to incubation with compound **16.** After rinsing with fresh medium (3 × 1.0 mL) to remove unbound conjugates, confocal images were acquired using a laser scanning confocal microscopy (FV 1000, Olympus) by excitation at 559 nm (yellow diode laser) and emission at 618 nm.

4.3.3. Binding affinity and competition or blocking study in LNCaP cells

LNCaP cells were seeded in T-75 flasks and were grown for 72 h. After 95% confluency, cells were trypsinized and centrifuged to form a cell pellet. Flow cytometry buffer was prepared by mixing 1X DPBS (50 mL), 25 mM HEPES buffer (1 mL) and EDTA (84 mg) and sterile filtered prior to use. 75,000 LNCaP cells in 100 μL of the medium were suspended in each of the Eppendorf tubes. The fluorescent conjugate **16** (400 μL medium) was added to the cell suspension (100 μL) to a final concentration of 5 to 1000 nM and incubated for 1 h at 4 °C. The treated cell suspension in each tube was centrifuged and washed with ice cold FACS buffer (3 × 1 mL) and the LNCaP cell pellet was suspended in ice cold FACS buffer (1 mL) for flow cytometry analysis. The mean fluorescence intensity was measured for each sample concentration (10,000 events) using flow cytometer (LSR Fortessa, BD Biosciences).

For competition or blocking experiment, the cell suspension in each tube (75,000 cells in 100 μL medium) was treated with 100-fold excess 2-PMPA (final vol = 300 μL medium) and incubated for 2 h at 4 °C. After treatment with 2-PMPA, fluorescent conjugate **16** (300 μL medium) was added (final vol = 600 μL medium) to make final concentrations of 5 to 1000 nM in each tube and further incubated for 1 h at 4 °C. The treated cell suspension in all tubes were centrifuged and rinsed with ice cold FACS buffer (3 × 1 mL) and the LNCaP cell pellet was suspended in ice cold FACS buffer (1 mL) for flow cytometry analysis. The mean fluorescence intensity was measured for each sample concentration (10,000 events) using flow cytometer (LSR Fortessa, BD Biosciences). Experiment was performed in triplicates. A plot of mean fluorescence intensity (a.u.) versus concentration of the test article afforded a dissociation constant (K_D) value of 88 nM for the bioconjugate **16** in LNCaP cells. The method of non-linear regression analysis was employed assuming one-site specific binding during the calculation of K_D using GraphPad Prism 6.02 software.

Declaration of Competing Interest

There are no conflicts of interest to declare.

Acknowledgements

The authors are thankful to the Ministry of Human Resource Development (MHRD), Government of India, Council of Scientific and Industrial Research (CSIR), and Indian Institute of Technology Indore, Government of India for research funding and fellowships. We also thank Sophisticated Instrumentation Centre (SIC), IIT Indore for providing instrumentation facilities. We would like to acknowledge AICTE and UGC for financial assistance for molecular modelling software's at the School of Pharmacy, DAVV, Indore.

Appendix A. Supplementary material

Supplementary data to this article can be found online at https://doi.org/10.1016/j.bioorg.2019.103154. Copy of ^1H, ^{13}C NMR and mass spectra of compounds **7**, **9**, **10**, and analytical LC data of CYUE-Rhodamine B conjugate **16,** binding and internalization of CYUE-Rhodamine B conjugate **16** in $PSMA^+$ LNCaP cells at different concentrations.

References

[1] M.C.S. Wong, W.B. Goggins, H.H.X. Wang, F.D.H. Fung, C. Leung, S.Y.S. Wong, C.F. Ng, J.J.Y. Sung, Global incidence and mortality for prostate cancer: analysis of temporal patterns and trends in 36 countries, Eur. Urol. 70 (2016) 862–874, https://doi.org/10.1016/j.eururo.2016.05.043.
[2] R.L. Siegel, K.D. Miller, A. Jemal, Cancer statistics, CA cancer, J. Clin. 68 (2018) (2018) 7–30, https://doi.org/10.3322/caac.21442.
[3] J.L. Zeller, Grading of prostate cancer, JAMA 298 (2007) 1596.
[4] M.D. Chodak, P. Keller, H.W. Schoenberg, Assessment of screening for prostate cancer using the digital rectal examination, J. Urol. 141 (1989) 1136–1138, https://doi.org/10.1016/s0022-5347(17), 41192-x.

[5] M. Essink-Bot, H.J. de Koning, H.G.J. Nijs, W.J. Kirkels, P.J. van der Mass, F.H. Schroder, Short term effects of population-based screening for prostate cancer on health-related quality of life, J. Natl. Cancer Inst. 90 (1998) 925–931, https://doi.org/10.1093/jnci/90.12.925.
[6] M.M. Linn, R.A. Ball, A. Maradiegue, Prostate-specific antigen screening: friend or foe? Urol. Nurs. 27 (2007) 481–489.
[7] M.R. Bernsen, K. Kooiman, M. Segbers, F.W.B. van Leeuwen, M. de Jong, Biomarkers in preclinical cancer imaging, Eur. J. Nucl. Med. Mol. Imag. 42 (2015) 579–596, https://doi.org/10.1007/s00259-014-2980-7.
[8] M.C. Gong, S.S. Chang, M. Sadelain, N.H. Bander, W.D. Heston, Prostate specific membrane antigen (PSMA)-specific monoclonal antibodies in the treatment of prostate and other cancers, Cancer Metast. Rev. 18 (1999) 483–490.
[9] A. Ghosh, W.D. Heston, Tumor target prostate specific membrane antigen (PSMA) and its regulation in prostate cancer, J. Cell. Biochem. 91 (2004) 528–539, https://doi.org/10.1002/jcb.10661.
[10] J.R. Mesters, C. Barinka, W. Li, T. Tsukamoto, P. Majer, B.S. Slusher, J. Konvalinka, R. Hilgenfeld, Structure of glutamate carboxypeptidase II, a drug target in neuronal damage and prostate cancer, EMBO J. 25 (2006) 1375–1384, https://doi.org/10.1038/sj.emboj.7600969.
[11] S.A. Kularatne, K. Wang, H.K.R. Santhapuram, P.S. Low, Prostate-specific membrane antigen targeted imaging and therapy of prostate cancer using a PSMA inhibitor as a homing ligand, Mol. Pharm. 6 (2009) 780–789, https://doi.org/10.1021/mp900069d.
[12] S.A. Kularatne, Z. Zhou, J. Yang, C.B. Post, P.S. Low, Design, synthesis, and preclinical evaluation of prostate-specific membrane antigen targeted ^{99m}Tc-radioimaging agents, Mol. Pharm. 6 (2009) 790–800, https://doi.org/10.1021/mp9000712.
[13] S.R. Banerjee, Z. Chen, M. Pullambhatla, A. Lisok, J. Chen, R.C. Mease, M.G. Pomper, Preclinical comparative study of ^{68}Ga-labeled DOTA, NOTA, and HBED-CC chelated radiotracers for targeting PSMA, Bioconjug. Chem. 27 (2016) 1447–1455, https://doi.org/10.1021/acs.bioconjchem.5b00679.
[14] X. Yang, R.C. Mease, M. Pullambhatla, A. Lisok, Y. Chen, C.A. Foss, Y. Wang, H. Shallal, H. Edelman, A.T. Hoye, G. Attardo, S. Nimmagadda, M.G. Pomper, [^{18}F]-Fluorobenzoyllysinepentanedioic acid carbamates: new scaffolds for positron emission tomography (PET) imaging of prostate-specific membrane antigen (PSMA), J. Med. Chem. 59 (2016) 206–218, https://doi.org/10.1021/acs.jmedchem.5b01268.
[15] S.R. Banerjee, M. Pullambhatla, C.A. Foss, S. Nimmagadda, R. Ferdani, C.J. Anderson, R.C. Mease, M.G. Pomper, ^{64}Cu-labeled inhibitors of prostate-specific membrane antigen for PET imaging of prostate cancer, Bioconjug. Chem. 57 (2014) 2657–2669, https://doi.org/10.1021/jm401921j.
[16] S.R. Banerjee, M. Pullambhatla, C.A. Foss, A. Falk, Y. Byun, S. Nimmagadda, R.C. Mease, M.G. Pomper, Effect of chelators on the pharmacokinetics of ^{99m}Tc-labeled imaging agents for the prostate-specific membrane antigen (PSMA), J. Med. Chem. 56 (2013) 6108–6121, https://doi.org/10.1021/jm400823w.
[17] Y. Chen, M. Pullambhatla, S.R. Banerjee, Y. Byun, M. Stathis, C. Rojas, B.S. Slusher, R.C. Mease, M.G. Pomper, Synthesis and biological evaluation of low molecular weight fluorescent imaging agents for the prostate-specific membrane antigen, Bioconjug. Chem. 23 (2012) 2377–2385, https://doi.org/10.1021/bc3003919.
[18] S.R. Banerjee, M. Pullambhatla, Y. Byun, S. Nimmagadda, G. Green, J.J. Fox, A. Horti, R.C. Mease, M.G. Pomper, ^{68}Ga-labeled inhibitors of prostate-specific membrane antigen (PSMA) for imaging prostate cancer, J. Med. Chem. 53 (2010) 5333–5341, https://doi.org/10.1021/jm100623e.
[19] C.J. Choy, X. Ling, J.J. Geruntho, S.K. Beyer, J.D. Latoche, B. Langton-Webster, C.J. Anderson, C.E. Berkman, ^{177}Lu-labeled phosphoramidate–based PSMA inhibitors: the effect of an albumin binder on biodistribution and therapeutic efficacy in prostate tumor–bearing mice, Theranostics 7 (2017) 1928–1939, https://doi.org/10.7150/thno.18719).
[20] S. Dannoon, T. Ganguly, H. Cahaya, J.J. Geruntho, M.S. Galliher, S.K. Beyer, C.J. Choy, M.R. Hopkins, M. Regan, J.E. Blecha, L. Skultetyova, C.R. Drake, S. Jivan, C. Barinka, E.F. Jones, C.E. Berkman, H.F. VanBrocklin, Structure-activity relationship of ^{18}F-labeled phosphoramidate peptidomimetic prostate-specific membrane antigen (PSMA)-targeted inhibitor analogues for PET imaging of prostate cancer, J. Med. Chem. 59 (2016) 5684–5694, https://doi.org/10.1021/acs.jmedchem.5b01850.
[21] K. Graham, R. Lesche, A.V. Gromov, N. Böhnke, M. Schäfer, J. Hassfeld, L. Dinkelborg, Georg Kettschau, Radiofluorinated derivatives of 2– (phosphonomethyl)pentanedioic acid as inhibitors of prostate specific membrane antigen (PSMA) for the imaging of prostate cancer, J. Med. Chem. 55 (2012) 9510–9520, https://doi.org/10.1021/jm300710j.
[22] S.E. Lapi, H. Wahnishe, D. Pham, L.Y. Wu, J.R. Nedrow-Byers, T. Liu, K. Vejdani, H.F. VanBrocklin, C.E. Berkman, E.F. Jones, Assessment of an 18F-labeled phosphoramidate peptidomimetic as a new prostate-specific membrane antigen-targeted imaging agent for prostate cancer, J. Nucl. Med. 50 (12) (2009) 2042–2048, https://doi.org/10.2967/jnumed.109.066589.
[23] S.A. Boppart, R. Richards-Kortum, Point-of-care and point-of-procedure optical imaging technologies for primary care and global health, Sci. Transl. Med. 6 (2014) 1–12, https://doi.org/10.1126/scitranslmed.3009725.
[24] A. Pandit, S. Sengupta, M.A. Krishnan, R.B. Reddy, R. Sharma, C. Venkatesh, First report on 3D–QSAR and molecular dynamics based docking studies of GCPII inhibitors for targeted drug delivery applications, J. Mol. Struct. 1159 (2018) 179–192, https://doi.org/10.1016/j.molstruc.2018.01.059.
[25] E. Al-Momani, N. Malik, H.-J. Machulla, S.N. Reske, C. Solbach, Radiosynthesis of [18F]FEt-tyr-urea-Glu ([18F]FEtTUG) as a new PSMA ligand, J. Radioanal. Nucl. Chem. 295 (2013) 2289–2294, https://doi.org/10.1007/s10967-012-2293-x.
[26] Z. Novakova, K. Wozniak, A. Jancarik, R. Rais, Y. Wu, J. Pavlicek, D. Ferraris, B. Havlinova, J. Ptacek, J. Vavra, N. Hin, C. Rojas, P. Majer, B.S. Slusher, T. Tsukamoto, C. Barinka, Unprecedented binding mode of hydroxamate-based inhibitors of glutamate carboxypeptidase II: structural characterization and biological activity, J. Med. Chem. 59 (2016) 4539–4550, https://doi.org/10.1021/acs.jmedchem.5b01806.
[27] C. Barinka, Z. Novakova, N. Hin, D. Bím, D.V. Ferraris, B. Duvall, G. Kabarriti, R. Tsukamoto, M. Budesinsky, L. Motlova, C. Rojas, B.S. Slusher, T.A. Rokob, L. Rulíšek, T. Tsukamoto, Structural and computational basis for potent inhibition of glutamate carboxypeptidase II by carbamate-based inhibitors, Bioorg. Med. Chem. 27 (2019) 255–264, https://doi.org/10.1016/j.bmc.2018.11.022.
[28] A.E. Machulkin, Y.A. Ivanenkov, A.V. Aladinskaya, M.S. Veselov, V.A. Aladinskiy, E.K. Beloglazkina, V.E. Koteliansky, A.G. Shakhbazyan, Y.B. Sandulenko, A.G. Majouga, Small-molecule PSMA ligands. Current state, SAR and perspectives, J. Drug Target 24 (2016) 679–693, https://doi.org/10.3109/1061186X.2016.
[29] S. Sengupta, M.A. Krishnan, P. Dudhe, R.B. Reddy, B. Giri, S. Chattopadhyay, C. Venkatesh, Novel solid-phase strategy for the synthesis of ligand-targeted fluorescent-labelled chelating peptide conjugates as a theranostic tool for cancer, Beilstein J. Org. Chem. 14 (2018) 2665–2679, https://doi.org/10.3762/bjoc.14.244.
[30] A.X. Zhang, R.P. Murelli, C. Barinka, J. Michel, A. Cocleaza, W.L. Jorgensen, J. Lubkowski, D.A. Spiegel, A remote arene-binding site on prostate specific membrane antigen revealed by antibody-recruiting small molecules, J. Am. Chem. Soc. 132 (2010) 12711–12716, https://doi.org/10.1021/ja104591m.